Coherent excitation energy transfer of meso-meso linked porphyrin array

ARTICLE · JANUARY 2007

DOI: 10.1109/CLEOPR.2007.4391783

4 AUTHORS, INCLUDING:

Dongho Kim

Yonsei University

499 PUBLICATIONS **13,545** CITATIONS

SEE PROFILE

Eunji Sim

Yonsei University

62 PUBLICATIONS **843** CITATIONS

SEE PROFILE

Coherence Length Determination of *meso*−*meso* Linked Porphyrin Arrays Based on Forward−Backward Pair Trajectory Analysis

Myeongwon Lee,[†] Heeyoung Kim,[†] Dongho Kim,*[,†,‡] and Eunji Sim*[,†]

Department of Chemistry and Institute for Nano-Bio Molecular Assemblies, and Center for Ultrafast Optical Characteristic Control, Yonsei University, 134 Sinchondong Seodaemungu, Seoul 120-749, Korea

Received: October 15, 2007; Revised Manuscript Received: March 5, 2008

We investigated the excitation energy transfer process of *meso*−*meso* linked zinc(II) porphyrin arrays using the on-the-fly filtered propagator path integral method. Details of the dynamics such as coherence length of a porphyrin array are estimated by analysis of the characteristics of forward−backward pair trajectories. Upon examination of the convergence of the reduced density matrix with respect to the subset of Hilbert space trajectories, we determine the number of porphyrin units that form collective coherent states, that is, the coherence length. Simulation results show that the coherence length of zinc(II) porphyrin arrays is up to 4 units, which agrees excellently with experimental observations. On the other hand, the energy bias provided by the energy-accepting 5,15-bisphenylethynylated zinc(II) porphyrin reduces the degree of coherence which becomes negligible for an array with more than for porphyrin units. Considering conformational inhomogeneity, we found that the experimentally determined coherence length is the result of electronic and environmental influence rather than the structure disorder. Temperature dependence is also discussed.

1. Introduction

Photosynthesis in nature begins with absorption of photons by light-harvesting antenna complexes, which are molecular aggregates consisting of peptides, chlorophylls, and carotenoids. The major function of a light-harvesting antenna complex is to funnel the energy with high efficiency to the reaction center in which primary charge separation takes place.[1–3] Recently, numerous artificial molecular architectures mimicking natural photosynthesis have intensively been explored in experiments, as well as in theoretical studies, to characterize and, in turn, to control optical properties of artificial photosynthesis.[4–7] In particular, Z*n* porphyrin molecular assemblies have been successfully synthesized that consist of *meso*−*meso* linked *n* units of orthogonal zinc(II) porphyrin arrays. To store the excitation energy, Z*n*A porphyrin arrays which have a 5,15-bisphenylethynylated porphyrin acceptor linked via a 1,4-phenylene spacer at the *n*th *meso*-carbon of Z*n* have also been characterized.[8] Figure 1 compares structures of Z*n* and Z*n*A, where *n* zinc(II) porphyrin units are orthogonal to each other. For unidirectional energy transfer from photoexcited donor array (Z*n*) to the energy acceptor (A), the triple-bond linkage (ethynylated) at two *meso* positions of the acceptor porphyrin moiety has elongated π-conjugation pathway leading to the lowering of the excited electronic state of the acceptor. Owing to the weak electronic interactions between ground states of Z*n* and A, it is possible to excite Z*n* selectively by tuning the excitation wavelength to be resonance with the Q-band of Z*n* and to observe the excitation energy transfer (EET) within the system using transient absorption spectroscopy.[4,8–10]

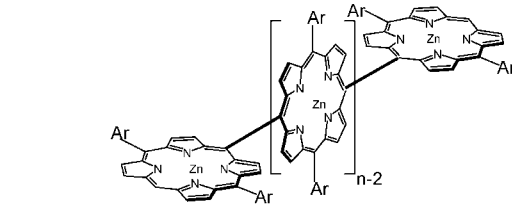

Ar=3.5-dioctyloxyphenyl

(a)

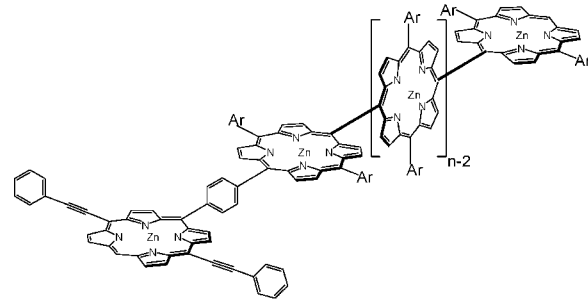

(b)

Figure 1. Porphyrin array (a) Z*n* and (b) Z*n*A systems, where *n* denotes the number of porphyrin donor units.

At the molecular level, the EET mechanism depends on the degree of coherence, that is, coherence length, within artificial photonic devices. Theoretical estimation on the coherence length for the wild type B850 light-harvesting antenna complex has been performed by various approaches. Coherence length of 4 Bacteriochlorophylls has been estimated empirically by Kimura and Kakitani[11–13] and with the use of Redfield theory by Kühn and Sundström.[14] On the other hand, Ray and Makri used the

* To whom correspondence should be addressed. E-mail: esim@yonsei.ac.kr (E.S.); dongho@yonsei.ac.kr (D.K.). Fax: +82-2-364-7050.
† Department of Chemistry and Institute for Nano-Bio Molecular Assemblies.
‡ Center for Ultrafast Optical Characteristic Control.

10.1021/jp709995u CCC: $40.75
Published on Web 05/21/2008

imaginary-time path integral simulations and estimated the coherence length as about 2 at room temperature.[15]

In this work, we aim to determine the coherence length of the EET process of artificial photonic arrays Z*n* and Z*n*A from $n = 2$ to 12 by means of EET pathway analysis rather than empirical or statistical approaches using the *real-time* path integration, combined with reduced trajectory spaces. For the propagation of the reduced density matrix of the EET process, the on-the-fly filtered propagator functional path integral (OFPF-PI) method is used, which is based on the Feynman and Vernon's influence functional formalism on a system coupled to a bath.[16–20] It has been shown that the convergence with respect to reduced trajectory spaces, which are a subset of all possible Hilbert space trajectories with particular forward−backward path deviation (FBPD), allows determining the number of electronic states that form collective coherent states, that is, coherence length.[21,22]

The article is organized as follows: In Section 2, we discuss the OFPF-PI formalism focusing on the correlation of forward and backward pathway with respect to the degree of coherence. Section 3 is devoted to the determination of the coherence length of Z*n* and Z*n*A arrays through the analysis into the quantum mechanical pair trajectories and to compare simulated results with experimental observations. Concluding remarks appear in Section 4.

2. Reduced Trajectory Space Path Integration

Because the EET dynamics is observed in solution phase, the energy transfer system, and a dissipative environmental bath should be considered. By assuming a weak bilinear interaction between an M state system and bath that consists of Q explicit harmonic modes, the total Hamiltonian is written as

$$H = H_s(s) + \sum_{j=1}^{Q}\left\{\frac{1}{2}M_j\dot{x}_j^2 + \frac{1}{2}M_j\omega_j^2 x_j^2\right\} - \sum_{j=1}^{Q} c_j x_j \sum_{k=1}^{M} \tilde{s}_k |u_k\rangle\langle u_k| \tag{1}$$

where $|u_k\rangle$ stands for an electronic state with corresponding grid point $\tilde{s}_k$, while M_j, ω_j, and x_j are the mass, harmonic frequency, and coordinate, respectively, of the jth bath mode that is coupled to the system with a coupling constant c_j. To study the transfer dynamics, we consider the reduced density matrix which is defined as

$$\tilde{\rho}(t) = Tr_b[e^{-iHt/\hbar}\rho(0)e^{iHt/\hbar}] \tag{2}$$

Here, $\rho(0)$ is the initial system−bath density matrix and $e^{-iHt/\hbar}$ is the forward-time propagator, while $e^{iHt/\hbar}$ is the backward-time propagator. Note that, unlike the wave function propagation, the density matrix propagation requires pair trajectories of forward and backward pathways.

To estimate the degree of coherence, we consider correlation between electronic states through analysis of contributing transfer pathways. For a given boundary condition, there are a large numbers of allowed quantum mechanical trajectories. Therefore contributions of all the possible trajectories should be counted for accurate dynamics. Previously, however, it was shown that only a fraction of possible trajectories indeed contribute significantly to the dynamics and that the vast majority of trajectories can be ignored without losing numerical accuracy.[19]

The relationship between states plays a significant role for the contribution of each pair trajectory, and thus, not all possible quantum mechanical pair trajectories contribute equally to the overall dynamics. Discretization of the reduced density matrix with the integration time step $\Delta t = t/N$ rewrites eq 2 as

$$\tilde{\rho}(t) = \sum_{k_0^{\pm}=1}^{M}\sum_{k_1^{\pm}=1}^{M}\cdots\sum_{k_N^{\pm}=1}^{M}\prod_{j=1}^{N-1}\left\{\langle u_{k_j^+}|e^{-iH_s\Delta t/\hbar}|u_{k_{j-1}^+}\rangle\langle u_{k_{j-1}^-}|e^{iH_s\Delta t/\hbar}|u_{k_j^-}\rangle\right\}\times \langle u_{k_N^+}|e^{-iH_s\Delta t/\hbar}|u_{k_{N-1}^+}\rangle\langle u_{k_{N-1}^-}|e^{iH_s\Delta t/\hbar}|u_{k_N^-}\rangle\times\langle u_{k_0^+}|\tilde{\rho}(0)|u_{k_0^+}\rangle\times \exp\left\{-\frac{1}{\hbar}\sum_{j=0}^{N}\sum_{j'=0}^{j}(\tilde{s}_{k_j^+}-\tilde{s}_{k_j^-})\left(\eta_{k_jk_{j'}}\tilde{s}_{k_{j'}^+}-\eta^*_{k_jk_{j'}}\tilde{s}_{k_{j'}^-}\right)\right\} \tag{3}$$

with the influence coefficients, $\eta_{k_jk_{j'}}$, that represent the nonlocal bath memory strength between time points t_j and $t_{j'}$.[23] In particular, the exponential term in eq 3 is called the influence functional.[16] As appeared in eq 3, integrands depend on the FBPD, $(\tilde{s}_{k_j^+} - \tilde{s}_{k_j^-})$.

Suppose the total trajectory space **C** includes all possible pair trajectories of the Hilbert space of M local excited states. Reduced trajectory space $\mathbf{C_m}$ is defined such that $\mathbf{C_m}$ includes trajectories whose FBPD does not exceed m sites at any time. Figure 2 schematically illustrates the relationship between the FBPD and the degree of coherence. Suppose the shaded area in Figure 2 represents a strongly coherent domain within a given EET system. When both of the forward and backward pathways are within the shaded area shown in Figure 2a, which means that the pair trajectory is composed of strongly coherent electronic states, the overall correlation within the pair trajectory is significant. Therefore the corresponding integrand in eq 3, that is, the contribution to the path integration, is large in magnitude. On the other hand, the pair trajectory in Figure 2b includes interactions between incoherent states so that it can be discarded in the path integration without loss of accuracy. In other words, for the case of Figure 2, three local states among four electronic states are strongly coherent such that the $\mathbf{C_2}$ reduced trajectory space guarantees inclusion of most of significantly correlated pair trajectories, and thus, path integration over the $\mathbf{C_2}$ space will give rise to the converged $\tilde{\rho}(t)$. Indeed, we previously showed that the average FBPD and its distribution of sorted pathways have close relationship to the degree of coherence on a quantitative basis.[21]

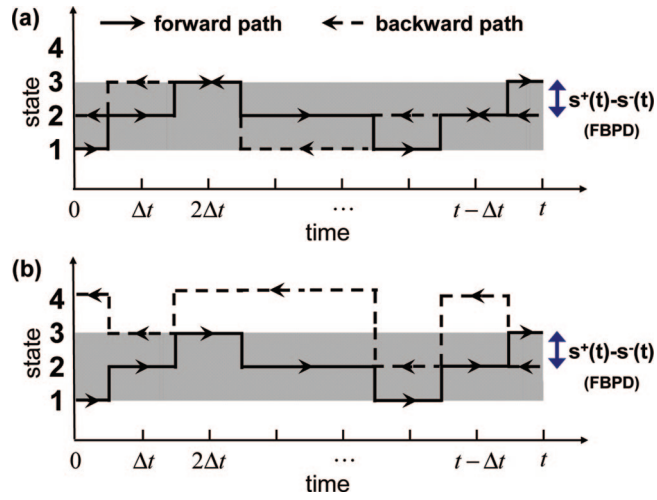

Figure 2. Typical trajectories in (a) $\mathbf{C_2}$ and (b) $\mathbf{C_3}$ reduced trajectory space. The shaded area represents strong coherence starting from the donor (1) state. States within the shades are strongly correlated; therefore, the trajectory a has large contribution to the transfer process, and the trajectory b can be discarded in path integration without losing numerical accuracy.

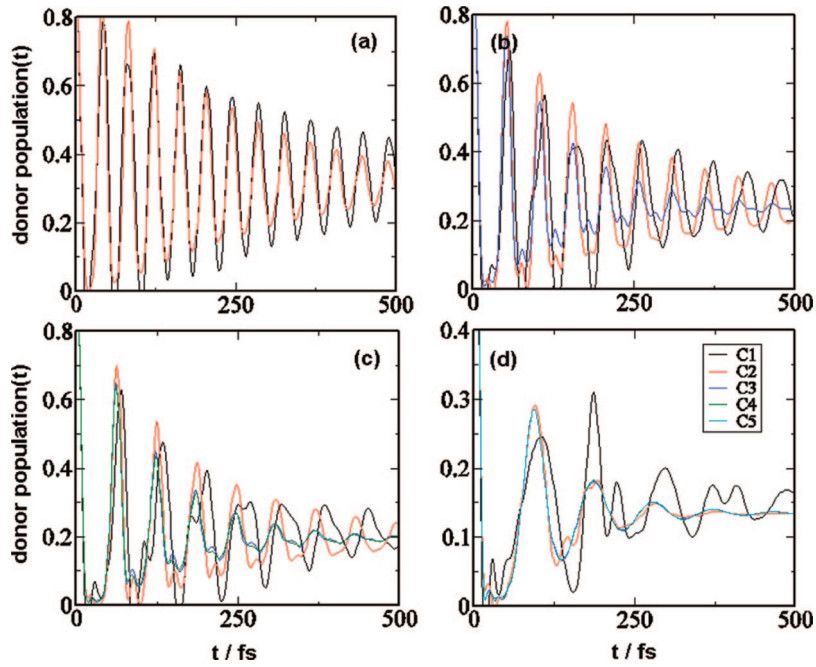

Figure 3. Time evolution of site energy population of the first donor state for Z*n* arrays at room temperature with respect to the reduced trajectory space used in path integration of eq 3. The propagation time step and the bath memory time are arbitrarily chosen to be $\Delta t = 1.75$ fs and $\tau_m = 8.75$ fs, respectively: (a) Z*3*, (b) Z*4*, (c) Z*5*, and (d) Z*12*.

TABLE 1: Potential Parameters for the Excitation Energy Transfer[a]

ΔE_{DA}	V_{DD}	V_{DA}	λ_{DD}	λ_{DA}	ω_c [300 K]	ω_c [77 K]
−1600	570	29	50	1576	400	100

[a] Units are in cm^{-1}.

The recently developed OFPF-PI approach systematically generates the pair trajectories and allows sorting of contributing pair trajectories without any statistical means. Therefore, the OFPF-PI method propagates eq 2 iteratively, and thus, exploration of an individual pair trajectory can be performed. The OFPF-PI is ideal to perform reduced trajectory space path integration employing a systematic path generation and the on-the-fly filtering algorithm.

In summary of this section, determination of the coherence length of an *M*-state EET system can be performed as follows: (1) Starting from $\mathbf{C_1}$ up to $\mathbf{C}_{M-1}$ space, evaluate corresponding $\tilde{\boldsymbol{\rho}}(t;\mathbf{C_m})$ using OFPF-PI formalism. (2) Compare $\tilde{\boldsymbol{\rho}}(t;\mathbf{C_m})$ to determine smallest converged space. (3) Once smallest converged space $\mathbf{C_\Gamma}$ is determined, then the coherence length is equal to $\Gamma + 1$.

3. Results and Discussion

To model the EET process in the Z*n* system that is composed of *n* zinc(II) porphyrin units, the system is represented in terms of *n* equivalent local electronic excited states. Using the tight-binding model, in which each site in the system represents a local exciton state, the Z*n* system Hamiltonian has an $n \times n$ matrixform

$$\mathbf{H}_s = \begin{pmatrix} 0 & V_{DD} & 0 & \cdots & 0 \\ V_{DD} & 0 & V_{DD} & \cdots & \vdots \\ 0 & V_{DD} & \ddots & & 0 \\ \vdots & \vdots & & 0 & V_{DD} \\ 0 & \cdots & 0 & V_{DD} & 0 \end{pmatrix} \quad (4)$$

where V_{DD} is the donor−donor coupling constant and the energy of the porphyrin exciton is set zero. With the acceptor, for the Z*n*A system, the $(n + 1) \times (n + 1)$ system Hamiltonian matrix is given by

$$\mathbf{H}_s = \begin{pmatrix} 0 & V_{DD} & 0 & \cdots & 0 \\ V_{DD} & 0 & V_{DD} & \cdots & \vdots \\ 0 & V_{DD} & \ddots & & 0 \\ \vdots & \vdots & & 0 & V_{DA} \\ 0 & \cdots & 0 & V_{DA} & E_{DA} \end{pmatrix} \quad (5)$$

with V_{DA} being the donor−acceptor coupling constants. The energy difference between the donor and acceptor electronic states is denoted as E_{DA}. While the interactions between the donor S_1 states are rather strong ($V_{DD} = 570$ cm^{-1}), the donor−acceptor coupling is weak ($V_{DA} = 29$ cm^{-1}) because of the separation by phenyl group between the donor and acceptor.[4,8] From the absorption spectra of Z*n*A, the energy difference between the donor and acceptor is estimated as $E_{DA} = -1600$ cm^{-1}.[4] To represent the system−bath interaction, we assumed 50 cm^{-1} for donor−donor and 1576 cm^{-1} for donor−acceptor reorganization energy, respectively.[24] Because the bath is composed of semi-infinite number of modes, it is advantageous to use the spectral density instead of explicit coupling constants.

Convergence of eq 3 with respect to the reduced trajectory space integration is shown in Figure 3 for Z*n* systems. The first donor state is excited, and the population relaxation is followed. As shown in Figure 3a, for Z*3*, population relaxation obtained using $\mathbf{C_1}$ and $\mathbf{C_2}$ (full) space substantially differs, indicating that the full pair trajectory space should be taken into account to obtain accurate transfer dynamics because the entire porphyrin array is coherent. Similar behavior is observed in Figure 3b for Z*4*, therefore we can conclude that up to four porphyrin units are strongly coherent. Furthermore, Figure 3c and d shows that the simulated

TABLE 2: Coherence Lengths and Converging Reduced Trajectory Spaces for Z*n* System at Room Temperature

array	Z*3*	Z*4*	Z*5*	Z*6*	Z*7*	Z*12*	Z*8*[a]
$\langle\lvert\tilde{\rho}(\mathbf{C_2})-\tilde{\rho}(\mathbf{C_1})\rvert\rangle$	0.05204	0.09274	0.09590	0.08206	0.06467	0.04525	0.18547
$\langle\lvert\tilde{\rho}(\mathbf{C_3})-\tilde{\rho}(\mathbf{C_2})\rvert\rangle$		0.04623	0.03736	0.02129	0.01055	0.00730	0.05315
$\langle\lvert\tilde{\rho}(\mathbf{C_4})-\tilde{\rho}(\mathbf{C_3})\rvert\rangle$			0.00546	0.00311	0.00137	0.00106	0.01502
$\langle\lvert\tilde{\rho}(\mathbf{C_5})-\tilde{\rho}(\mathbf{C_4})\rvert\rangle$				0.00003	0.00020	0.00010	0.00482
$\langle\lvert\tilde{\rho}(\mathbf{C_6})-\tilde{\rho}(\mathbf{C_5})\rvert\rangle$					3.6×10^{-5}	1.8×10^{-5}	0.00190
$\langle\lvert\tilde{\rho}(\mathbf{C_7})-\tilde{\rho}(\mathbf{C_6})\rvert\rangle$							0.00041
coherence length	Z*3*	Z*4*	Z*4*	Z*4*	Z*4*	Z*4*	Z5
converged **C** space	$\mathbf{C_2}$	$\mathbf{C_3}$	$\mathbf{C_3}$	$\mathbf{C_3}$	$\mathbf{C_3}$	$\mathbf{C_3}$	$\mathbf{C_4}$

[a] At 77 K.

population no longer alters by integrating on larger reduced trajectory spaces than $\mathbf{C_3}$. This agrees excellently with experimentally observed coherence length of 4.5 that was determined according to the dependence of radiative decay rate constants on the number of porphyrin units.[25,26]

Previously, we suggested that the coherence length in linear Zn(II) porphyrin arrays ($n > 4$) is 4−5 porphyrin units based on the radiative decay rate constants measured by steady-state (fluorescence quantum yield) and time-resolved fluorescence decay measurements.[26,27] By normalization of the fluorescence spectra of Z*4*, Z*6*, Z*8*, and Z*12* measured in THF solvent, their spectral shapes are similar yet slightly different in the intensities in the lowest vibronic bands.[8] More importantly, the fluorescence spectrum of Z*4* is much different from those of Z*1*, Z*2*, and Z*3*. On the basis of these spectral features, the fluorescence spectra of both Z*4* and Z*12* originate from the cooperative oscillation of four porphyrin units. However, the Z*4* units in Z*12* fluoresce somewhat differently from the Z*4* array because of the adjacent porphyrin units in Z*12*. Thus the spectral similarity and difference in Z*4* and Z*12* imply that 4−5 porphyrin units in Z*12* oscillating cooperatively act as an excitation energy hopping unit along the linear array. In addition, the empirical formula of the coherence length (N_c) for a one-dimensional linear array system developed by Kakitani et al. is as follows:[11,13]

$$N_c = 1.38 + 1.33\frac{V}{\gamma} \tag{6}$$

By using eq 6 with the estimated exciton coupling $V = V_{DD} = 570\ \text{cm}^{-1}$ and the homogeneous broadening $\gamma = 250\ \text{cm}^{-1}$, the coherence length $N_c = 4.5$ and ∼4 were obtained in the absence and the presence of inhomogeneity, respectively.[28]

Owing to the continuous decrease of the coherence with distance, it is sometimes ambiguous to determine the coherence length. Therefore, we defined a convergence parameter and a cutoff value such that the convergence of integration results can be determined on the equal footing for all cases: the convergence parameter is a time average of the difference between the donor population results obtained from $\mathbf{C_m}$ and $\mathbf{C_{m+1}}$ space, given as

$$\chi = \langle\lvert\tilde{\rho}(\mathbf{C_{m+1}};t) - \tilde{\rho}(\mathbf{C_m};t)\rvert\rangle \tag{7}$$

where $\langle\ldots\rangle$ represents a time average. With this, the $\mathbf{C_m}$ space gives rise to the converged results where $\chi \leq 0.005$. At $\chi \approx 0.005$, the donor population shows negligible discrepancy at the scales shown in Figure 3. The convergence parameter for Z*n*

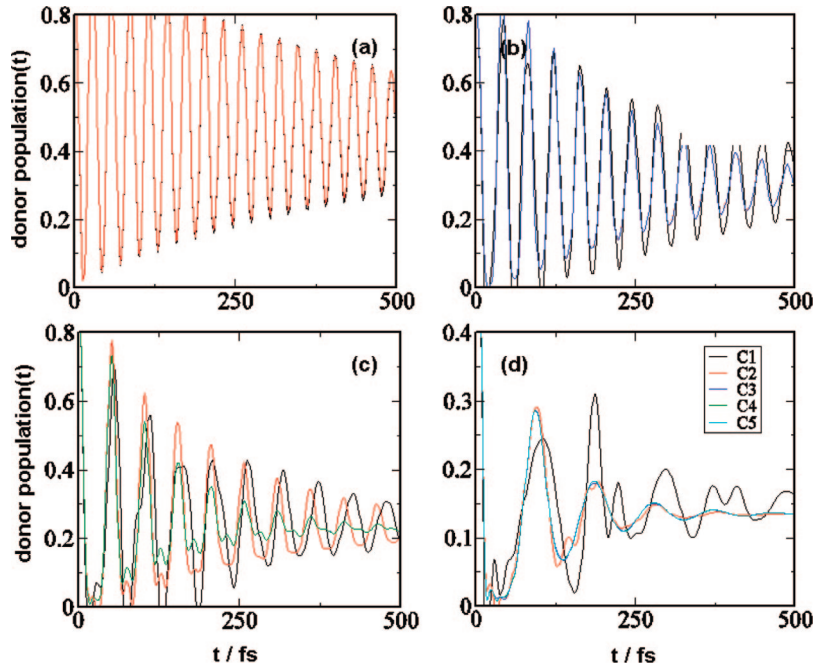

Figure 4. Same as Figure 3 for Z*n*A arrays. The propagation time step and the bath memory time are arbitrarily chosen to be $\Delta t = 1.75$ fs and $\tau_m = 8.75$ fs, respectively: (a) Z2A, (b) Z*3*A, (c) Z*4*A, and (d) Z*12*A.

TABLE 3: Coherence Lengths and Converging Reduced Trajectory Spaces for Z*n*A System at Room Temperature

array	Z*2*A	Z*3*A	Z*4*A	Z*5*A	Z*6*A	Z*12*A
$\langle\lvert\tilde{\rho}(\mathbf{C}_2)-\tilde{\rho}(\mathbf{C}_1)\rvert\rangle$	0.00395	0.05184	0.09157	0.09492	0.08221	0.04763
$\langle\lvert\tilde{\rho}(\mathbf{C}_3)-\tilde{\rho}(\mathbf{C}_2)\rvert\rangle$		0.00020	0.04679	0.03699	0.02119	0.00755
$\langle\lvert\tilde{\rho}(\mathbf{C}_4)-\tilde{\rho}(\mathbf{C}_3)\rvert\rangle$			2.3×10^{-5}	0.00542	0.00310	0.00106
$\langle\lvert\tilde{\rho}(\mathbf{C}_5)-\tilde{\rho}(\mathbf{C}_4)\rvert\rangle$				9.7×10^{-7}	0.00033	0.00010
$\langle\lvert\tilde{\rho}(\mathbf{C}_6)-\tilde{\rho}(\mathbf{C}_5)\rvert\rangle$					5.7×10^{-8}	1.8×10^{-5}
coherence length	Z*2*	Z*3*	Z*4*	Z*4*	Z*4*	Z*4*
converged **C** space	$\mathbf{C_1}$	$\mathbf{C_2}$	$\mathbf{C_3}$	$\mathbf{C_3}$	$\mathbf{C_3}$	$\mathbf{C_3}$

arrays is summarized in Table 2. On the basis of the convergence parameter cutoff, 4 porphyrin units are strongly coherent.

In Figure 4, influence of the energy bias on the coherence length is clearly visible. For the Z*2*A array, as in Figure 4a, the integration results from $\mathbf{C_1}$ and $\mathbf{C_2}$ spaces are almost identical and $\chi = 0.00395$ in Table 3. It shows that, although the two donor porphyrin units are strongly coherent, correlation between the donor array and the acceptor is very weak because of the energy bias despite the short distance between them. Similar behavior is also observed in Figure 4b and c for Z*3*A and Z*4*A, that donor populations obtained from $\mathbf{C_{n-1}}$ and $\mathbf{C_n}$ integration are identical in both cases with $\chi = 0.00020$ and 2.3 ± 10^{-5}, respectively. It suggests that the entire donor arrays be coherent up to Z4A. For even more extended arrays from Z*5*A to Z*12*A, the donor population for Z*n*A ($n \geq 4$) converges to $\mathbf{C_3}$ space that is identical to the case of Z*n* ($n \geq 4$) arrays. The convergence parameters are also summarized in Table 3.

Experimentally determined dephasing time of a monomer *x*,*y* transition dipole is shorter than 200 fs, while that of the dimer is measured to be roughly 200 fs because of the mixing of the monomer *x*,*y* transition dipole and the interaction between porphyrins.[29] Measuring the dephasing time is not only difficult experimentally, but it is also challenging in theoretical studies based on empirical and effective models. Because the reduced density matrix of EET process provides the time evolution of electronic states, it allows deduction of the dephasing time of various lengths of porphyrin arrays on a quantitative basis. We performed the time constant analysis for Z*n* systems and estimated the dephasing time to be approximately 190, 100, and 50 fs, respectively, for Z*3*, Z*4*, and Z*12* arrays. As expected, the dephasing time was observed to decrease with array dimension. Note that the dynamic properties of EET should be estimated from converged reduced density matrix, while the data presented in Figure 3 based on arbitrarily chosen integration conditions to illustrate advantages of pathway analysis.

For the model systems in eq 4 and Figure 4, the Z*n* array is supposed to have a perfectly linear geometry without any structural inhomogeneity. The structural disorder with Zn arrays in a dihedral angle, $\varphi_{\text{dihedral}}$, is expected to be within 20 degrees at room temperature.[8] To explore the structural inhomogeneity, we constructed structurally disordered Z*8* arrays in which $\varphi_{\text{dihedral}} = 70$ and 90 degrees are randomly mixed. The coupling constant between adjacent porphyrin units at $\varphi_{\text{dihedral}} = 70$ was determined as 540 cm^{-1} on the basis of the spectral splitting in UV−vis absorption spectra.[30,31] Four dihedral angle disordered configurations were simulated as presented in Figure 5 and Table 4. In both configurations, it is observed that the use of $\mathbf{C_3}$ space gives rise to the converged results as for the case of perfectly orthogonal configuration. Excellent agreement with experimentally observed coherence length in the absence and presence of the dihedral angle disorder suggests that the consistency of the coherence length up to four porphyrin units should be mainly associated with the electronic and environmental effect rather than the structural inhomogeneity.

We also investigated temperature-dependent coherence length for the case of Z*8* array. To mimic low-temperature effect of

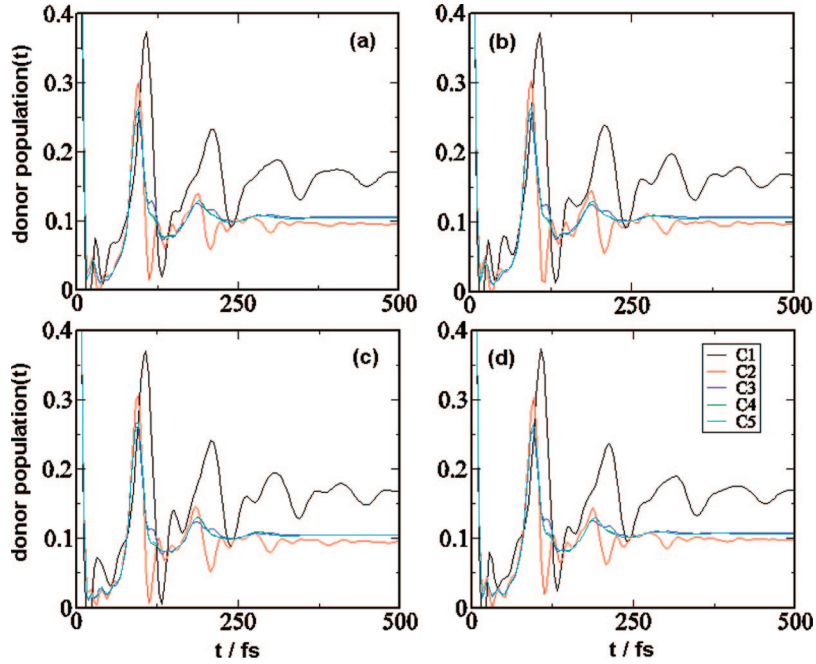

Figure 5. Same as Figure 3 for structurally disordered Z*8* arrays. The propagation time step and the bath memory time are arbitrarily chosen to be $\Delta t = 4$ fs and $\tau_m = 20$ fs, respectively. Structural disorder in the dihedral angle between adjacent porphyrin units are introduced as (a) 90−70−90−90−90−70−90°, (b) 90−70−90−70−90−90−70°, (c) 90−90−70−90−90−90−70°, and (d) 90−70−70−90−90−70−90°.

TABLE 4: Coherence Lengths and Converging Reduced Trajectory Spaces for Dihedral Angle Disordered Z*8* Configurations at Room Temperature

$\varphi_{\text{dihedral}}$	90−70−90−90−90−70−90	90−70−90−70−90−90−70	90−90−70−90−90−90−70	90−70−70−90−90−70−90
$\langle\lvert\tilde{\rho}(C_2)-\tilde{\rho}(C_1)\rvert\rangle$	0.06531	0.06396	0.06685	0.06264
$\langle\lvert\tilde{\rho}(C_3)-\tilde{\rho}(C_2)\rvert\rangle$	0.01341	0.01360	0.01318	0.01304
$\langle\lvert\tilde{\rho}(C_4)-\tilde{\rho}(C_3)\rvert\rangle$	0.00238	0.00254	0.00208	0.00222
$\langle\lvert\tilde{\rho}(C_5)-\tilde{\rho}(C_4)\rvert\rangle$	0.00024	0.00027	0.00028	0.00024
coherence length	*Z4*	*Z4*	*Z4*	*Z4*
converged **C** space	$\mathbf{C_3}$	$\mathbf{C_3}$	$\mathbf{C_3}$	$\mathbf{C_3}$

the bath fluctuations at 77 K compared to room temperature, the cutoff frequency of the spectral density was reduced from 400 to 100 cm^{-1}. Figure 6 and Table 2 show that the population converges from $\mathbf{C_5}$ space such that the coherence length of the *Zn* array is extended up to 6 porphyrin units upon lowering the temperature. Note that fluctuations of bath modes slow down at low temperatures and thus dissipative influence of the environment to the EET system weakens resulting in longer coherence length. Successful representation of the temperature dependency implies that the computational scheme used in this work adequately describes the EET process in the condensed medium and allows exploring the detailed transport dynamics.

4. Concluding Remarks

We applied a novel tool to evaluate the coherence length of the EET processes of *Zn* and *Zn*A systems. Using the OFPF-PI formalism combined with the reduced trajectory spaces, one can sort out contributing pair trajectories and analyze characteristics of the transfer without empirical parameters. To estimate the coherence length of the *Zn* system, we employed multistate models in which each site represents an explicit local exciton state, which is coupled to a dissipative environment. Coherence between states was determined upon examining the convergence of the reduced density matrix with respect to the reduced trajectory space integration that includes pair trajectories with predetermined maximum FBPD. Furthermore, dynamical characteristics of the decoherence, that is, the dephasing time, can also be measured which is absent in empirical studies and effective models.[13–15]

For coherent migration dominated processes in *meso*−*meso* linked porphyrin units, simulation results showed that coherence length of porphyrin arrays is up to four units that agrees excellently with experimental observation. It was also found that the energy bias by the acceptor weakens the coherence between donor and acceptor units. Nevertheless, the influence of the acceptor bias becomes negligible for arrays with more than 4 donor porphyrin units. Electronic and environmental configuration dominates the EET process. The structural disorder is insignificant in the determination of the coherence between porphyrin units. Temperature dependence was also investigated. The coherence length becomes longer at low temperatures because of slow fluctuation bath modes.

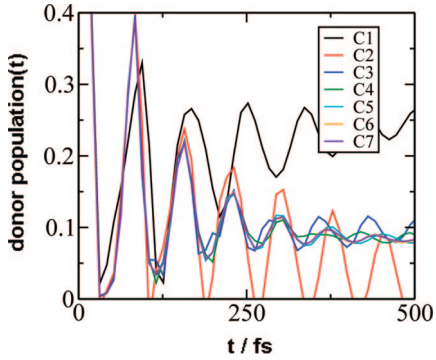

Figure 6. Same as Figure 4 for Z*8* array at 77 K. The propagation time step and the bath memory time are arbitrarily chosen to be Δt = 10.5 fs and τ_m = 42 fs, respectively.

Acknowledgment. This work was supported by the Korea Science and Engineering Foundation (KOSEF-R01-2007-000-11831-0, E.S.) and by the Korea Research Foundation (KRF-2006-312-C00200, E.S.) and the Star Faculty Program (D.K.) of the Ministry of Education and Human Resources Development (MEHRD). H.K. and M.L. thank fellowship of the BK21 program from MEHRD. ES also appreciates Donghyun Kim for fruitful and valuable discussion.

References and Notes

(1) Hu, X. C.; Ritz, T.; Damjanovic, A.; Schulten, K. *J. Phys. Chem. B* **1997**, *101*, 3854.
(2) Sundstrom, V.; Pullerits, T.; van Grondelle, R. *J. Phys. Chem. B* **1999**, *103*, 2327.
(3) Renger, T.; May, V.; Kuhn, O. *Phys. Rep.* **2001**, *343*, 138.
(4) Aratani, N.; Cho, H. S.; Ahn, T. K.; Cho, S.; Kim, D.; Sumi, H.; Osuka, A. *J. Am. Chem. Soc.* **2003**, *125*, 9668.
(5) Guldi, D. M. *Chem. Soc. Rev.* **2002**, *31*, 22.
(6) Sim, E.; Makri, N. *J. Phys. Chem. B* **1997**, *101*, 5446.
(7) Nakamura, Y.; Hwang, I. W.; Aratani, N.; Ahn, T. K.; Ko, D. M.; Takagi, A.; Kawai, T.; Matsumoto, T.; Kim, D.; Osuka, A. *J. Am. Chem. Soc.* **2005**, *127*, 236.
(8) Kim, Y. H.; Jeong, D. H.; Kim, D.; Jeoung, S. C.; Cho, H. S.; Kim, S. K.; Aratani, N.; Osuka, A. *J. Am. Chem. Soc.* **2001**, *123*, 76.
(9) Piet, J. J.; Taylor, P. N.; Anderson, H. L.; Osuka, A.; Warman, J. M. *J. Am. Chem. Soc.* **2000**, *122*, 1749.
(10) Rhee, H.; Joo, T.; Aratani, N.; Osuka, A.; Cho, S.; Kim, D. *J. Chem. Phys.* **2006**, 125.
(11) Kimura, A.; Kakitani, T.; Yamato, T. *J. Phys. Chem. B* **2000**, *104*, 9276.
(12) Kimura, A.; Kakitani, T. *J. Phys. Chem. B* **2003**, *107*, 14486.
(13) Kakitani, T.; Kimura, A. *J. Phys. Chem. A* **2002**, *106*, 2173.
(14) Kühn, O.; Sundstrom, V. *J. Chem. Phys.* **1997**, *107*, 4154.
(15) Ray, J.; Makri, N. *J. Phys. Chem. A* **1999**, *103*, 9417.
(16) Feynman, R. P.; Vernon, F. L. *Ann. Phys.* **2000**, *281*, 547.
(17) Sim, E. *J. Chem. Phys.* **2001**, *115*, 4450.
(18) Sim, E. *J. Phys. Chem. B* **2004**, *108*, 19093.
(19) Sim, E.; Makri, N. *Chem. Phys. Lett.* **1996**, *249*, 224.
(20) Makri, N.; Makarov, D. E. *J. Chem. Phys.* **1995**, *102*, 4600.
(21) Sim, E.; Kim, H. *J. Phys. Chem. B* **2006**, *110*, 13642.
(22) Kim, H.; Lee, M.; Sim, E. *Bull. Korean Chem. Soc.* **2007**, *28*, 607.
(23) Sim, E.; Makri, N. *Comput. Phys. Commun.* **1997**, *99*, 335.
(24) Ko, D.; Kim, H.; Park, J. H.; Kim, D.; Sim, E. *Bull. Korean Chem. Soc.* **2005**, *26*, 1505.
(25) Ha, J. H.; Cho, H. S.; Song, J. K.; Kim, D.; Arataini, N.; Osuka, A. *ChemPhysChem* **2004**, *5*, 57.
(26) Ahn, T. K.; Yoon, Z. S.; Hwang, I. W.; Lim, J. K.; Rhee, H.; Joo, T.; Sim, E.; Kim, S. K.; Aratani, N.; Osuka, A.; Kim, D. *J. Phys. Chem. B* **2005**, *109*, 11223.
(27) Park, M.; Cho, S.; Yoon, Z. S.; Aratani, N.; Osuka, A.; Kim, D. *J. Am. Chem. Soc.* **2005**, *127*, 15201.
(28) Kim, D.; Osuka, A. *J. Phys. Chem. A* **2003**, *107*, 8791.
(29) Cho, H. S.; Rhee, H.; Song, J. K.; Min, C. K.; Takase, M.; Aratani, N.; Cho, S.; Osuka, A.; Joo, T.; Kim, D. *J. Am. Chem. Soc.* **2003**, *125*, 5849.
(30) Yoshida, N.; Ishizuka, T.; Osuka, A.; Jeong, D. H.; Cho, H. S.; Kim, D.; Matsuzaki, Y.; Nogami, A.; Tanaka, K. *Chem.—Eur. J.* **2003**, *9*, 58.
(31) Kim, D.; Osuka, A. *J. Phys. Chem. A* **2003**, *107*, 8791.

JP709995U